PAPER

Design, modeling and 3D printing of a personalized cervix tissue implant with protein release function

To cite this article: Chenjia Zhao *et al* 2020 *Biomed. Mater.* **15** 045005

IOP Publishing Biomed. Mater. 15 (2020) 045005 https://doi.org/10.1088/1748-605X/ab7b3b

Biomedical Materials

PAPER

RECEIVED
11 November 2019

REVISED
3 February 2020

ACCEPTED FOR PUBLICATION
28 February 2020

PUBLISHED
29 May 2020

Design, modeling and 3D printing of a personalized cervix tissue implant with protein release function

Chenjia Zhao[1,2,3], Zitong Wang[1,2,3], Chen Hua[6], Jingyuan Ji[1,2,3], Zhenzhen Zhou[1,2,3], Yongcong Fang[1,2,3], Ding Weng[1,2,5], Lu Lu[6], Yuan Pang[1,2,3,7] and Wei Sun[1,2,3,4,7]

[1] Biomanufacturing Center, Dept. of Mechanical Engineering, Tsinghua University, Beijing 100084, People's Republic of China
[2] Biomanufacturing and Rapid Forming Technology Key Laboratory of Beijing, Beijing 100084, People's Republic of China
[3] Overseas Expertise Introduction Center for Discipline Innovation, Tsinghua University, Beijing 100084, People's Republic of China
[4] Department of Mechanical Engineering, Drexel University, Philadelphia, PA 19104, United States of America
[5] State Key Laboratory of Tribology, Tsinghua University, Beijing 100084, People's Republic of China
[6] Key Laboratory of Medical Molecular Virology (MOE/NHC/CAMS), School of Basic Medical Sciences, Fudan-Jinbo Functional Protein Joint Research Center, Fudan University, Shanghai, People's Republic of China
[7] Yuan Pang and Wei Sun contributed equally and should be co-corresponding author.

E-mail: pangyuan31@mail.tsinghua.edu.cn **and** weisun@mail.tsinghua.edu.cn

Keywords: 3D printing, cervical implant, protein release, anti-HPV, polyurethane

Abstract

Cervical cancer induced by human papillomavirus (HPV) causes severe morbidity worldwide. Although cervical conization has been widely accepted as the most conventional surgery against cervical cancer, tissue defects and high recurrence rates have a significant negative impact on women's mental and physical health. Herein we developed an implantable, personalized cervical implant with drug release function using 3D printing technology. The cervical implant was designed in cone-shape with hieratical porous structures according to the clinical data, 3D-printed using polyurethane by low-temperature deposition manufacturing (LDM), and finished by lyophilization. Anti-HPV protein was loaded into the porous structure under negative pressure afterwards. Elastic biomedical polyurethane and the porous structure ensured that these cervical implants were equipped with tailored mechanical properties comparable to physiological cervix tissue. Cytotoxicity and cytocompatibility tests indicated that these 3D-printed cervical implants supported cell adhesion and growth. More importantly, the cervical implants with regulated pores could help to quantitatively control the loading and release of anti-HPV protein to inhibit dissociative viruses near the cervix validly. As a result, the 3D-printed cervical implants in the present study showed considerable potential for use as functional tissue implants against HPV infection after cervical conization.

1. Introduction

Cervical cancer, 91% induced by the human papillomavirus (HPV), is among the most common malignant tumors treated by gynecologists, with secondary mortality just lower than that of breast cancer [1]. A total of 460 000 new cases are identified each year worldwide from which approximately 250 000 people die [2, 3]. The most common and effective treatment remains extensive transabdominal hysterectomy (conization, figure 1(a)), from which the survival rate can reach 87%–92% [4]. However, the cervical conization removes part of the cervix tissue, resulting in tissue deficiency in the cervical structure, increasing the risk of postoperative infertility, miscarriage and premature birth [5–7] and representing a great threat to the mental and physical health of patients. In addition, conization surgery also results in patients being prone to recurrence of cervical cancer, due to the dissociative HPV virus in the vagina not being completely eliminated [8]. Therefore, preservation of a patient's reproductive and physiological function following effective inhibition for HPV remains a problem that urgently requires a solution in obstetrics, gynecology and related disciplines.

In recent years, as the discipline of tissue engineering has developed, the use of biomaterials to construct

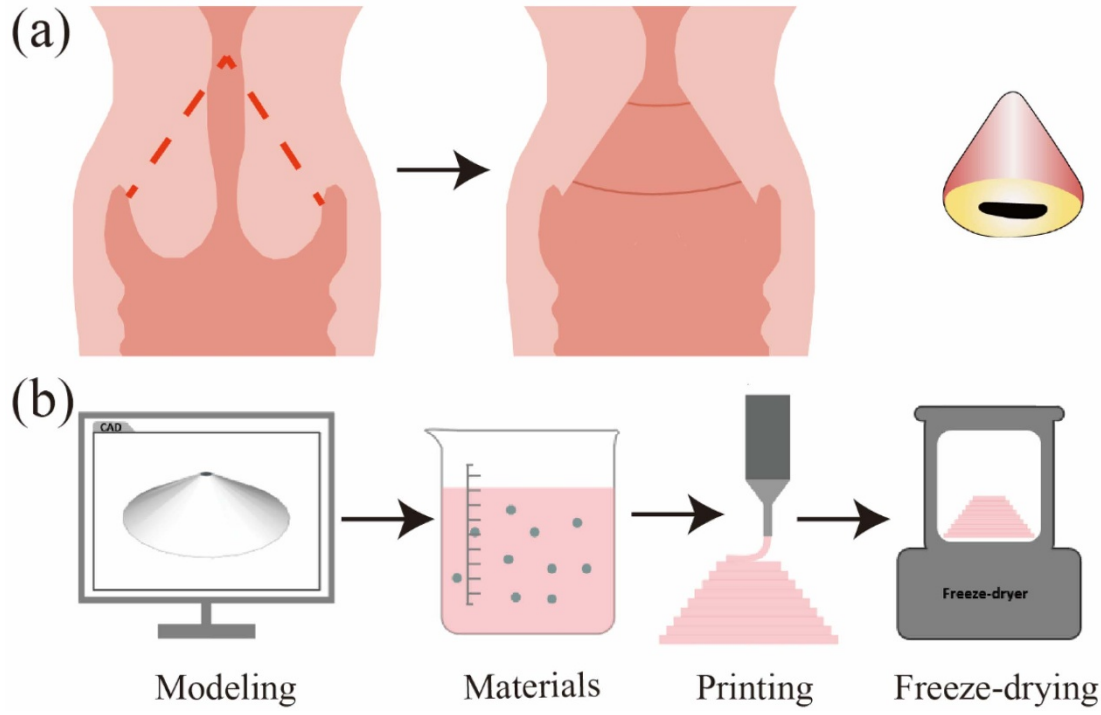

Figure 1. (a) Conization surgery; (b) a schematic of the printing system.

tissue substitutes has become a promising approach to repair and reconstruct defective tissues and organs. At present, large-scale animal experiments have demonstrated the reconstruction and repair of defects in structural tissues such as bone, cartilage, tendon and skin [9–12]. In order to achieve effective tissue regeneration, functional cytokines like growth factors and proteins are often incorporated into and *in vivo* controlled released from implanted tissue engineering scaffolds, which promote cell migration, proliferation and differentiation to repair the wound site [13]. Therefore, inoculation of anti-HPV drugs within properly designed cervical implants is a promising route towards tissue regeneration, functional preservation, and effective anti-HPV infection after cervical conization.

Among manufacturing methods used in tissue engineering, three-dimensional printing technology (3D printing) promises a potential approach to tissue or organ repair, due to its flexibility and precision based on the rapid prototyping of materials [14–17]. With the increased demand for personalized and precision medicine, 3D printing technology has attracted considerable attention [18, 19]. Personalized solid models, implants and assistive devices created by 3D printing can be effective in improving the success rate of surgery and postoperative rehabilitation [20–22]. By mimicking the structure of the physiological tissue, a customized implant achieved a perfect match between substitute and lesion in the patients, accomplishing the desired tissue repair effect [23]. Furthermore, by combining different functional 3D printing technologies with different types of biomaterial, it is possible to produce drug-loaded tissue implants with specific release profiles to match patient requirements and promote the therapeutic effect [24, 25]. These studies on 3D-printed drug-loaded constructs highlight a promising direction for improvements in the survival rate and functionality of tissue substitutes, providing a new strategy for clinical treatment [26, 27].

In view of the high recurrence rate of cervical cancer and the problem of partial tissue defect after the surgical conization, we herein proposed the construction of personalized cervical implants. By loading with the anti-HPV protein, the fabricated cervical implant could repair defected cervix as a soft tissue patch, as well as release anti-HPV protein to prevent virus infection. Due to its great flexibility, fast manufacturing and accuracy, 3D printing technology was employed in this study to reconstruct the personalized cervical biomimetic structure. We first designed and developed a computer model of the 3D reconstructed cervix tissue implant based on medical imaging data. An FDA-approved implantable biomaterial, polyurethane, was used as raw material for printing by a low temperature deposition (LDM) technology (figure 1(b)). Different from other 3D printing technologies, LDM technology fabricates structures rapidly soon after extrusion due to the low-temperature environment of −20 °C to −30 °C. The temperature transition during printing cause phase separation inside the printed construct, and by incorporating with freeze-drying technology, a porous

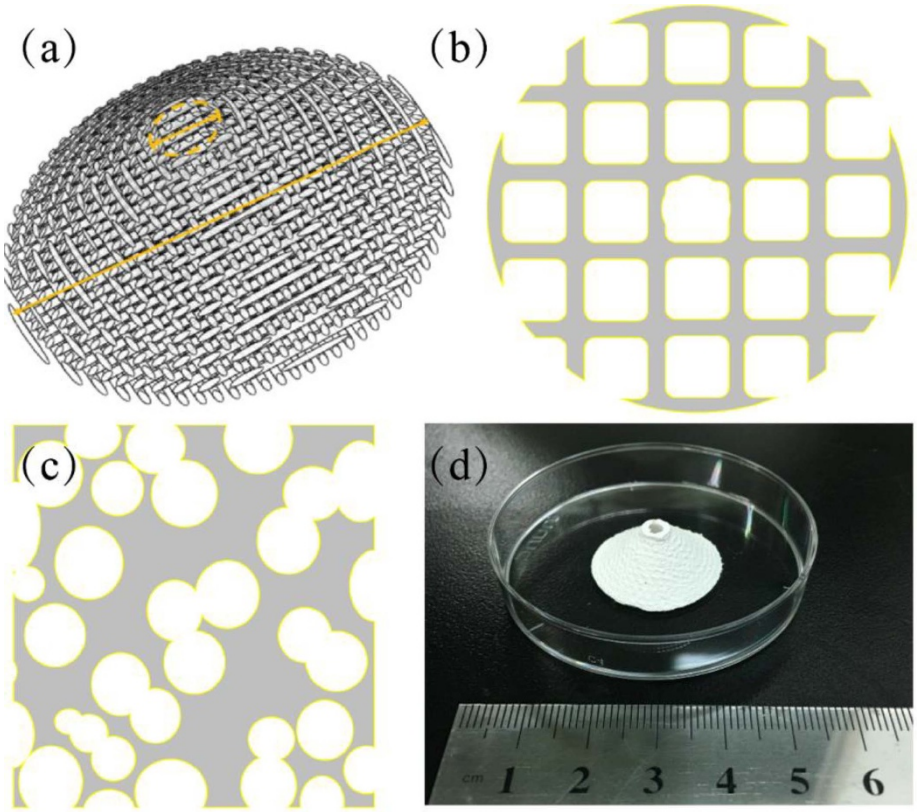

Figure 2. (a) 3D reconstruction of the defect cervical tissue in conization; (b) JB protein attached on the surface of macro-pores of the cervix implant; (c) JB protein attached on the surface of micro-pores of the cervix implant; (d) the cervical implant after lyophilization.

structure will be finally obtained [28]. These porous structures provide customized mechanical properties, as well as providing enlarged surface area for drug loading and releasing [29]. Mechanical characterization and biocompatibility tests demonstrated that printed cervical implants had mechanical properties comparable to the physiological cervix tissues with a biocompatible environment for cell adhesion and growth. Bovine β-lactoglobulin modified with 3-hydroxyphthalic anhydride, termed 'JB protein', able to block HPV virus infection [30–33], was used as a drug to inoculate the lyophilized cervical implant using a negative pressure loading technique. The porosity could quantitatively regulate protein dose loaded on the cervical implant and ultimately control protein release. These results suggest the promising role of current 3D-printed cervical constructs in both tissue repair and anti-HPV infection treatment, and demonstrate their potential towards personalized treatment in the future.

2. Materials and methods

2.1. General concept and design of the implantable cervix

2.1.1. Design of the cervix implant

In gynecological surgery, three types of cervical conization are performed depending on the infiltration of the cervical cancer [34]: type I resection (10 mm deep), type II resection (10–15 mm deep) and type III resection (15–25 mm deep) with a base diameter of approximately 30 mm. Another physiological feature for consideration is a hollow structure in the cervix, with a diameter of up to 8 mm which functions as a channel to eliminate secretions from the uterus [35]. Therefore, the cervical implant was designed as a conical structure 30 mm in diameter at its base. The height of the structure could be adjusted from 10–25 mm, corresponding to the three types of conization. A hollow channel 5 mm in diameter was created that vertically penetrated the construct, mimicking the *in vivo* cervical structure allowing excretion of uterine tissue endocrine fluid (figure 2(a)).

2.1.2. Porous structure for protein loading

In order to achieve the loading and rapid release of JB protein, the cervical implant was designed to have a multi-level porous structure. The 1st hierarchical pores were created due to wire spacing between the material filaments in extrusion-based 3D printing and the 2nd hierarchical pores were micro-pores generated through evaporation of the solvent during fabrication (figures 2(b) and (c)). The adjustable macropores in cervical implants could provide customized mechanical properties, whilst the micropores in the deposited filaments contributed to controlling

loading and releasing protein through enlarged surface area. For a cube of side length (a), fixed wire spacing (d) and wire diameter (D), macro-porosity η and surface area S could be calculated as follows [36]:

$$\eta_{\text{theoretical macroporosity}} = (1 - d/D) \times 100\% \quad (1)$$

$$S = \delta a^3 \left(1 - \eta_{\text{theoretical macroporosity}}\right) \quad (2)$$

where δ represents specific surface area. Wire spacing was set at 0.8 mm, 1.0 mm, 1.2 mm, 1.4 mm or 1.6 mm, with wire diameter fixed at 0.4 mm. The height of the cervix implant was fixed as 10 mm to replicate a type I conization resection to prove the concept. A 3D model of the construct was then generated using Mimics v10.01 3D reconstruction software and Creo computer-assisted design (CAD) modeling software.

2.2. Materials and cell preparation

JB protein was supplied by Jingbo Biological Pharmaceutical Co., Ltd. A stock solution was prepared in deionized water at a concentration of 26.9 mg ml^{-1}. Polyetherurethane (Zhejiang Huafeng Chemical Co., Ltd.) was selected as the raw material and prepared in 1,4-dioxane (12.5% w/v) for printing. Human umbilical vein endothelial cells (HUVECs) (China Infrastructure of Cell Line Resources, Beijing) were cultured in high glucose DMEM culture medium (Invitrogen) supplemented with 10% fetal bovine serum (FBS) (Hyclone), 1% nonessential amino acid solution (NEAA) (Gibco), 40 μU ml^{-1} insulin and 1% antibiotics (penicillin and streptomycin, Gibco) at 37 °C in a humidified atmosphere containing 5% CO_2. Hela cells (Cell Resources Center, IBMS, CAMS/PUMC, Beijing) were cultured in DMEM culture medium (Invitrogen) supplemented with 10% FBS (Hyclone), 1% NEAA (Gibco), and 1% antibiotics (penicillin and streptomycin, Gibco) at 37 °C in 5% CO_2. HPV pseudovirus were prepared by transfecting 293 T cells with a mixture of HPV16-L1/L2-expressing plasmid (p16sheLL) and pCLucf plasmid for HPV16 PsV, using VigoFect (Vigorous Biotechnology Corp.) [37].

2.3. Fabrication of the cervical implant via LDM

The cervical implant was fabricated using an LDM (SunP Biotech). During printing, polyurethane solution was molded into a filamentous structure by micro-extrusion through a nozzle at a temperature of −30 °C ~ −40 °C, which ensured that the polyurethane solution quickly solidified after extrusion. By combining 3D motion units, the cervical implant was then printed from the designed CAD model at a scan speed of 22 mm s^{-1}, jet speed of 0.01 mm s^{-1}, interlayer distance of 0.15 mm and nozzle diameter of 400 μm. The printed 3D construct was frozen at −80 °C for 24 h for further solidification followed by lyophilization in an Alpha 1–2 freeze dryer (Martin Christ GmbH, Osterode am Harz, Germany) for 48 h. 1,4-dioxane was sublimated during freeze-drying creating micropores in each printed filament of the construct.

2.4. Characterization of the printed 3D construct

2.4.1. Cytotoxicity testing of the polyurethane material and 3D-printed constructs

Polyurethane solution was poured into glass petri plates to form a uniform film after freeze-drying and cut into pieces. Cuboid structures 10 × 10 × 10 mm in size were printed for preparing extraction. According to the ISO Standard 10 993–12 [38], 4 ml complete culture medium for HUVECs was incubated with the polyurethane pieces and cuboid structures at 37 °C in 5% CO_2 for 24 h, and the extraction ratios were 3 cm^2 ml^{-1} and 0.1 g ml^{-1}, respectively. With the same processing, another two extracts were prepared using complete culture medium of Hela cells. Then the extract medium was transferred into the wells of a 96-well plate where HUVECs and Hela cells were respectively seeded at a density of 2.5×10^4 cells ml^{-1}. HUVECs and Hela cells cultured in normal medium represented as control and the cell-free culture medium represented the blank sample. After incubation for 96 h, cellular proliferation in each group was evaluated using a Cell Counting Kit-8 (CCK-8) for the characterization of cytotoxicity.

2.4.2. Cytocompatibility test of printed 3D construct

Mesh-like cuboid structures 10 × 10 × 1.6 mm in size were printed for cell compatibility testing. Suspensions of HUVECs and Hela cells at a density of 1×10^6 cells ml^{-1}, marked with PKH 67 (Sigma), were separately inoculated onto the constructs for 24 h then cell attachment observed using a laser-scanning confocal microscope (LSCM; LSM 710 META, Zeiss) to assess cytocompatibility of the printed 3D constructs.

2.4.3. Construct morphology (SEM observation and porosity measurement)

3D-printed constructs of different porosities were coated with gold-palladium (50 nm) and observed using a scanning electron microscope (SEM) (FEI Quanta 200, Czech Republic) for morphological evaluation. The porosity of the constructs was measured using a drainage method by immersing into 99% alcohol within a measuring cylinder. The original volume of alcohol was recorded as V_1, and the total volume after soaking the construct recorded as V_2. Following removal of the construct, the remaining volume of alcohol was recorded as V_3. The porosity (η) was calculated as follows:

$$\eta = \frac{V_1 - V_3}{V_2 - V_3} \times 100\%. \quad (3)$$

2.4.4. Mechanical properties of the printed 3D constructs

The compressive properties of the 3D-printed constructs of different porosities were tested by using an EnduraTEC ELF 3200 (Bose). Samples were blocks 11 × 11 × 5.5 mm. A force transducer measuring ±50 N was chosen in an unconstrained uniaxial compression test using a loading rate of 0.5 mm s^{-1}, a data acquisition rate of 4 s^{-1} and a maximum compression distance of 10% of the sample height.

Tensile properties were measured using an electronic universal material testing machine (Changchun Kecheng Experimental Instrument Research Institute). Pieces of polyurethane material, monofilaments and printed 3D constructs of different porosities were prepared for tensile testing. Samples were stretched at 20 mm min^{-1} until breaking and the elastic modulus recorded.

2.5. Protein loading and release

2.5.1. Surface treatment of printed constructs

The surface of the polyurethane material was oxidized by exposure to oxygen plasma using a Femto small-scale laboratory production plasma system (low-pressure plasma, Diener Electronics, Germany). The working gas was oxygen at a chamber pressure of 40–100 Pa. Two parameters, duration of irradiation (10 s–5 min) and plasma power (0–100 W), were measured to evaluate the effect of plasma treatment. Water contact angle tests were performed on the air-facing surfaces of samples using the sessile drop method to ascertain the most appropriate surface treatment conditions.

2.5.2. Protein loading and release

Prior to surface treatment, printed constructs were first immersed into 75% ethanol for 3 h, washed repeatedly with PBS three times then placed on a super-clean bench for UV sterilization for 30 min. After drying, the constructs were modified by exposure to oxygen plasma followed by immersion in 4 ml bovine beta-lactoglobulin solution for 24 h at negative pressure at room temperature.

Protein-laden cervical implants were transferred to 15 ml PBS on a shaker at 60 rpm to measure protein release over 20 h. After the protein release experiment, samples were dissolved in xylene to retrieve all remaining protein inside the constructs. The quantity of protein was quantified using a Micro BCA kit. The cumulative release of protein from the cervical implants was calculated by equation (4):

$$R_n = \frac{\left[V_e \sum_{k=1}^{n-1} C_k + V_0 C_n\right]}{\left[V_e \sum_{k=1}^{n-1} C_k + V_0 C_n + m_r\right]} \times 100\% \quad (4)$$

where R_n is the cumulative release of protein, V_e is the volume of each sample for analysis, C_k is the protein concentration in the release solution at the kth sampling, V_0 is the total volume of release solution and m_r the quantity of protein remaining on the cervical implant. Release profiles were fitted using the Weibull equation [39] as follows:

$$R_n = 100(1 - \exp\left(-(t/\tau)^d\right) \quad (5)$$

where t represents release time, τ represents the time after which 63.2% of the drug had been released and constant d represents the transport mechanism of the drug [40, 41].

2.5.3. Tests for inhibition against HPV pseudovirus [42, 43]

HeLa cells were seeded at the density of 1.5 × 10^4 cells in 100 μl of complete culture medium per well in a 96-well plate and cultured at 37 °C in 5% CO_2 overnight. The JB protein before and after the release was serially diluted using DMEM and incubated with 100 μl of HPV pseudovirus. The incubated mixture was then added to HeLa cells for culture at 37 °C in 5% CO_2 for 16 h. After replacement of the culture supernatants with free medium and culture for additional 72 h, cells were lysed for measurement of luciferase activity with the Dual-Luciferase® Reporter (DLR™) Assay System (Promega, Madison, WI, USA).

2.6. Statistical analysis

Researchers conducting the tests described above were blind to the identity of each sample. T-tests measuring means ± standard deviation of each group of data were compared using SPSS 11.0 software. Differences between results were analyzed using the Mann–Whitney test method and accepted as significant with $p \leq 0.05$.

3. Results

3.1. Characteristics of cervical implants

Based on 3D reconstruction models of the cervix, the printed cervical implants (wire spacing: 1200 μm) after lyophilization are displayed in figure 2(d). The height of the cervical implant was 8.350 ± 0.42 mm, diameter of the base 26.18 ± 1.69 mm and diameter of the hollow channel was 4.27 ± 0.31 mm, smaller than the original design, resulting from shrinkage caused by lyophilization.

Monofilaments were formed by stretching droplets ejected by the moving nozzles on the platform during the printing process. The measured diameters were slightly larger than the design parameter of 400 μm, possibly due to the larger droplets caused by surface tension. From a comparison of constructs of different wire spacing, the shape, size and distribution of macro-pores in constructs with a wire spacing of 1.2 mm, 1.4 mm and 1.6 mm were more uniform, as shown in figure 3. The size of micropores, providing adhesion surface for proteins which would undergo subsequent multi-level sustained release, in

Table 1. Porosity and sizes of macro-pores and micro-pores in cervical implants.

Wire spacing	Theoretical macro-porosity	Calculated total porosity (%)	Measured total porosity (%)	Macro-pore size (μm)	Micro-pore size (μm)
800 μm	50%	82.24 ± 2.44	83.95 ± 5.07	300.99 ± 53.83	3.82 ± 1.84
1000 μm	60%	85.78 ± 1.79	85.92 ± 2.25	407.66 ± 32.88	1.82 ± 1.86
1200 μm	66.7%	88.17 ± 1.49	87.83 ± 4.23	608.93 ± 65.94	2.68 ± 1.69
1400 μm	71.4%	89.83 ± 1.39	90.62 ± 1.29	721.42 ± 55.26	1.42 ± 0.79
1600 μm	75%	91.12 ± 1.22	92.31 ± 1.59	979.08 ± 42.06	3.08 ± 1.79

n = 6, p < 0.05, ANOVA, Tukey–Kramer test.

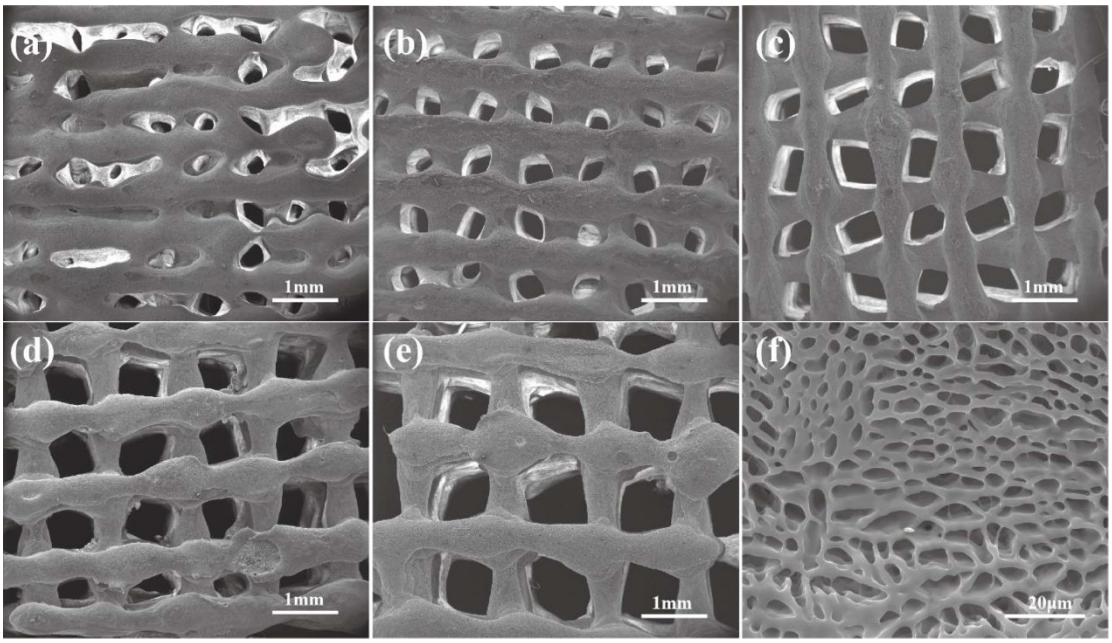

Figure 3. SEM images of cervical implants of different wire spacing. (a)–(e) Constructs with wire spacing of 0.8 mm, 1.0 mm, 1.2 mm, 1.4 mm, 1.6 mm, respectively; (f) micropores inside of the filaments.

the five cervical implant versions were all distributed below 10 μm. The microscopic surfaces of the constructs were analyzed using Image-Pro Plus 6.0 software. Microscopic porosity inside the constructs was 64.47 ± 4.88 %.

As suggested by conventional drainage measurements, the porosities of the cervical implants with the five wire spacing measurements were all greater than 80% and larger than the theoretical macro-porosity (table 1), due to the presence of micro-pores inside the constructs. The relationship between total porosity (η_{total}), macro-porosity ($\eta_{\text{macro-porosity}}$) and micro-porosity ($\eta_{\text{micro-porosity}}$) was described as follows:

$$\eta_{\text{total}} = 1 - \left(1 - \eta_{\text{macro-porosity}}\right) * \left(1 - \eta_{\text{micro-porosity}}\right). \quad (6)$$

For a micro-porosity of 64.47 ± 4.88 %, equation (6) could be calculated as:

$$\eta_{\text{total}} = (0.3553 \pm 0.0488)\,\eta_{\text{macro-porosity}} + (0.6447 \pm 0.0488). \quad (7)$$

Therefore, total porosity could be calculated, as the theoretical macro-porosity resulting from the wire spacing was known. As shown in table 1, there was no significant difference (P = 0.136) between measured total porosity and calculated total porosity, demonstrating that current fabrication process was reliable and effective in fabricating cervical implants with specific porosities.

3.2. Biomechanical analysis of printed constructs

According to the stress-strain curves shown in figure 4(a), the polyurethane materials had an elastic modulus of 6.92 MPa. These results demonstrate that the polyurethane had good elasticity and could be restored to their original shape following a large elastic deformation, ensuring the durability of the 3D-printed cervical implants. Elongation at break was greater than 400%, suggesting that it would not break easily after being subjected to a large deformation.

Analysis of the stress-strain curve indicated that printed polyurethane monofilaments had a good elasticity, with the elastic modulus at 3.016MPa, which would allow them to return to their original shapes after a large elastic deformation (figure 4(b)). Elongation at break was greater than 500%, indicating that it would not be easily broken when subjected

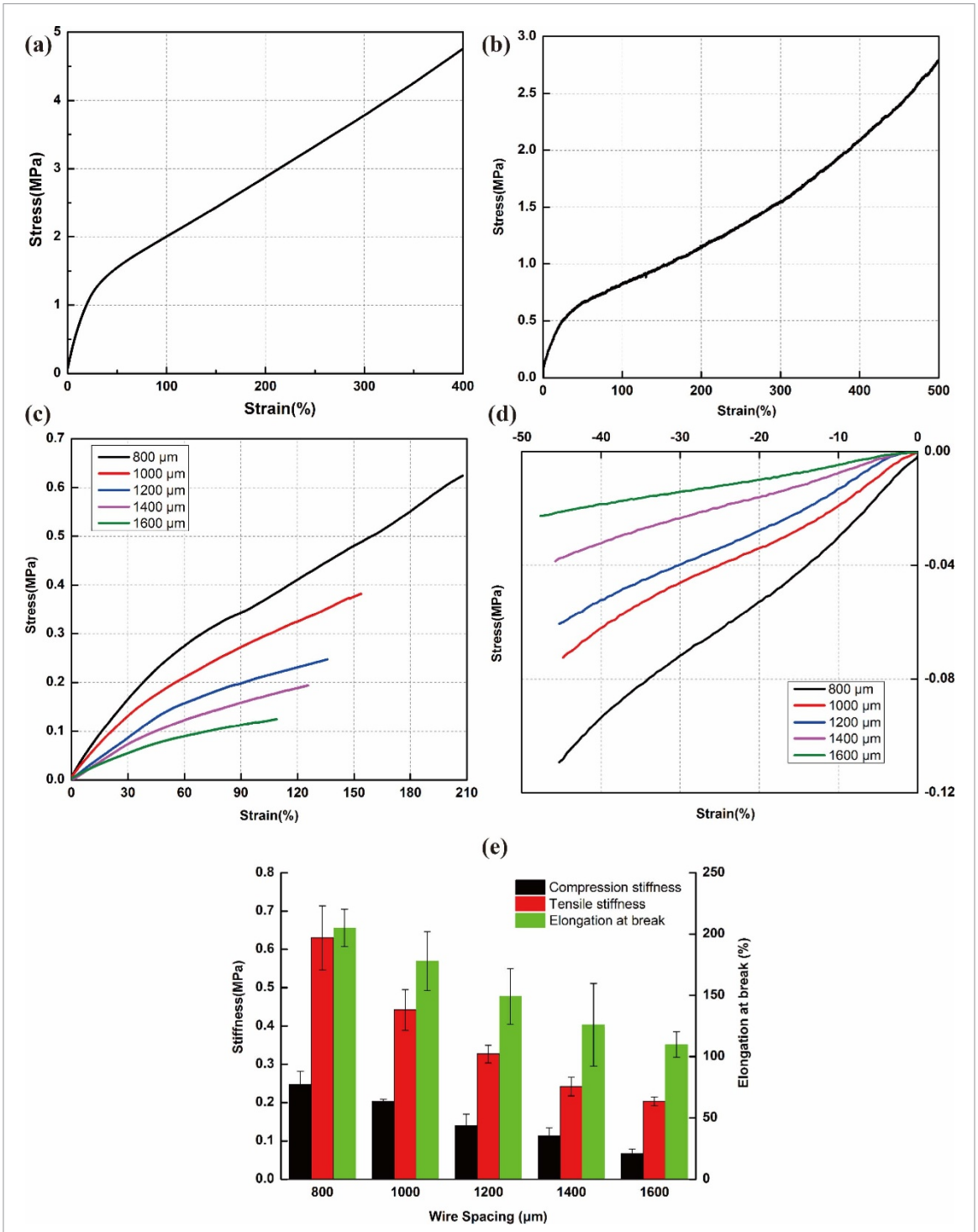

Figure 4. Stress–strain curves of biomechanical assay of polyurethane, printed polyurethane monofilament and printed constructs (a) stress–strain curve of a standard polyurethane tensile film with a thickness of 0.042 mm; (b) stress–strain curve of the polyurethane monofilament with a diameter of 0.4 mm and a length of 5 mm; (c) stress–strain curves of constructs (120 mm × 10 mm × 1.8 mm) with different wire spacing in tensile experiments; (d) stress–strain curves of constructs with different wire spacing in compression tests; (e) compression stiffness, tensile stiffness and elongation at break of printed 3D constructs ($p \leq 0.05$, $n = 3$) with different wire spacing.

to a large deformation. Compared with a cast polyurethane sample, printed polyurethane monofilaments were lyophilized and contained micro-pores along their length, resulting in them having a smaller elastic modulus, better elasticity and higher elongation, indicating that a polyurethane cervical implant with high levels of elasticity could be prepared using an LDM process.

As a type of woven mesh structure, the tensile properties of 3D-printed constructs are direction-specific, manifested as having a larger tension bearing capacity in the direction of its length compared with other directions. As displayed in the stress-strain curves, the stiffness of the five constructs was lower than 0.7 MPa, indicating that the constructs possessed excellent stretchability (figure 4(c)).

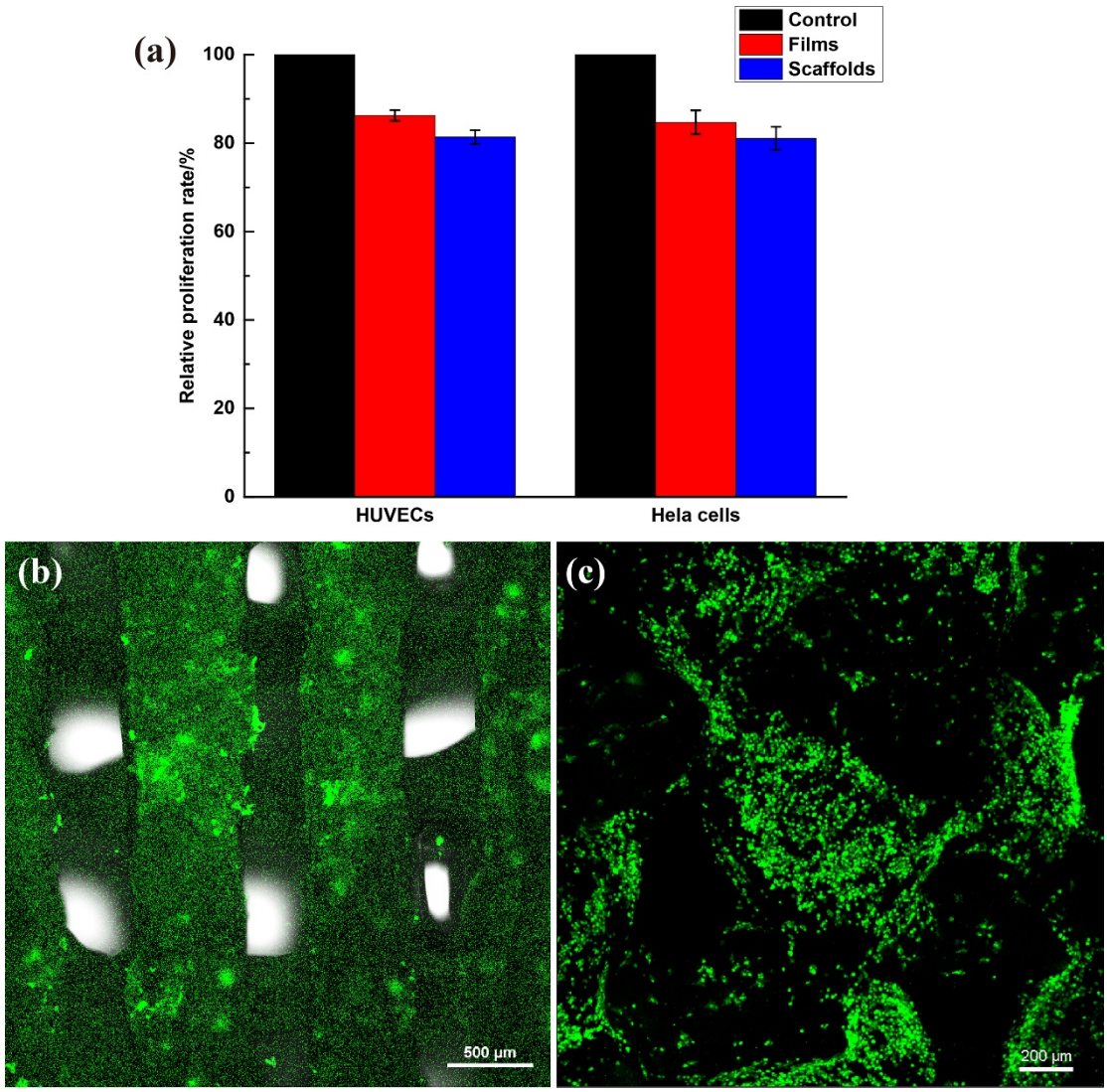

Figure 5. Results of biocompatibility test. (a) The relative proliferation rate of HUVECs and Hela cells cultured in extract of PU films and 3D-printed constructs ($p \leq 0.05$, $n = 3$); (b) constructs with wire spacing of 1.2 mm immersed in HUVECs suspension at a density of 1×10^6 cells ml^{-1}(marked with PKH67); (c) constructs with wire spacing of 1.2 mm immersed in Hela cell suspension at a density of 1×10^6 cells ml^{-1} (marked with PKH67).

As porosity increased, the stiffness and the elongation at break decreased, increasing stretchability.

Constructs were subjected to a compression test using a 10% deformation of the original height of the structure (figure 4(d)). The compression stiffness of the five types of construct were below 0.25 MPa in all cases, demonstrating that the compressibility of the constructs was appropriate and consistent with the results of porosity measurement. As structure porosity increased, stiffness decreased, resulting in an increase in compressibility and flexibility.

3.3. Cytotoxicity and cytocompatibility test

After culturing HUVECs and Hela cells for 96 h, proliferation in the 12 groups was evaluated using a CCK-8 by measuring absorbance in a microplate reader at a wavelength of 450 nm. The relative proliferation rates of HUVECs and Hela cells cultured in the extract of polyurethane film and 3D-printed constructs were all above 80%. The ISO 10993-5 guidelines state that materials causing a relative proliferation rate higher than 80% meet the standards for implants, demonstrating that the printed constructs caused little cytotoxicity and thus were suitable for cervical implantation.

The cytocompatibility tests were carried out by incubating HUVECs and Hela cells with the constructs in the same culture wells for 24 h, in order to observe whether the 3D-printed constructs are suitable for cell adhesion. Laser-scanning confocal micrographs showing cellular adhesion and cell morphology on printed 3D constructs are presented in figure 5(b). HUVECs and Hela cells were observed homogenously distributed on the constructs after 24 h of culture. These observations suggest that the 3D-printed constructs provide a biocompatible environment for adhesion and proliferation of HUVECs and Hela cells.

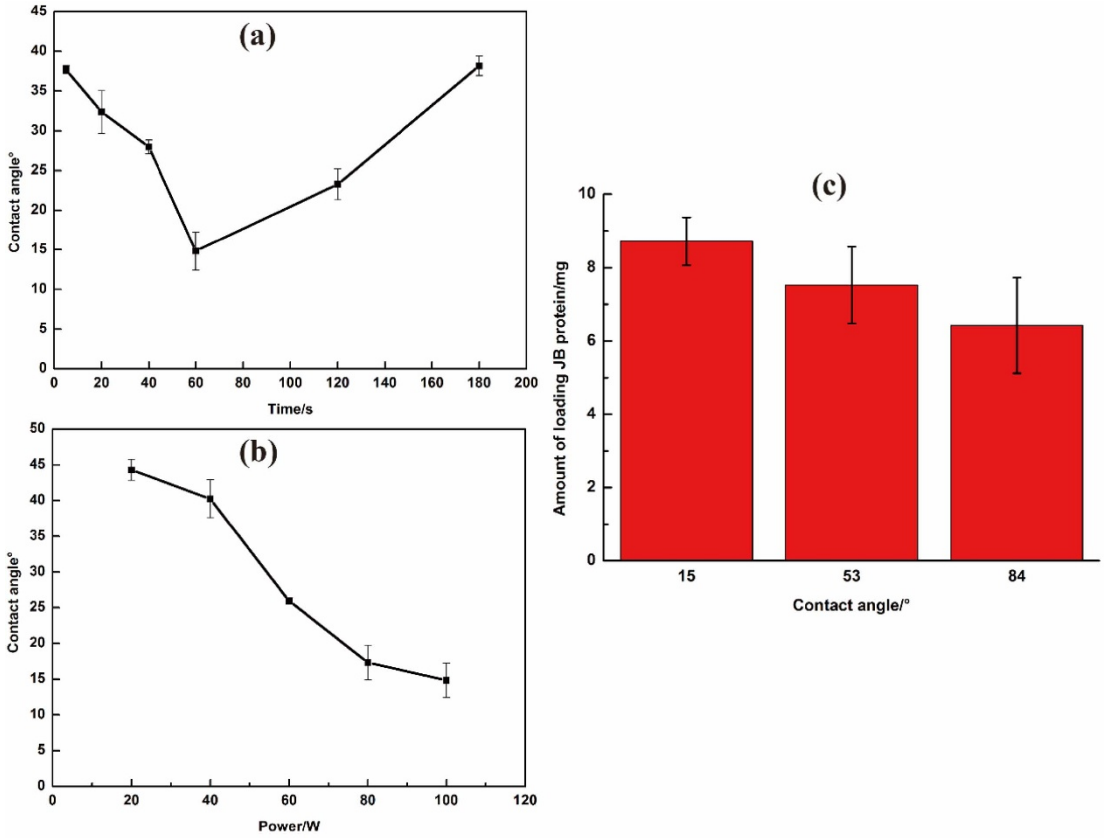

Figure 6. Optimization of surface treatment parameters. (a) Contact angle changes with processing time; (b) contact angle changes with power; (c) the amount of JB protein loading on polyurethane with different contact angles. ($p \leq 0.05$, $n = 3$).

3.4. Protein loading and release

3.4.1. Surface treatment for protein loading

The polyurethane films were surface treated to modify their hydrophilicity to explore the relationship between protein loading and polyurethane hydrophilicity. At a constant power of 100 W, a minimum water contact angle was obtained after a 1 min treatment (figure 6(a)). Subsequently, the water contact angle began to increase, possibly due to the etching effect of the plasma treatment. For a treatment duration of 1 min, contact angles for different plasma processing powers are displayed in figure 6(b). These results indicate that the water contact angle decreased as the power input increased, due to higher powers causing greater ionization of atoms and molecules resulting in greater surface modification of the film.

Protein loading experiments were performed on polyurethane materials with water contact angles of 15°, 53° and 84°, prepared using different surface treatment conditions. After 24 h, the quantity of protein loaded on each piece of polyurethane material was quantified by measuring the difference in protein concentration in the loading solution. The results shown in figure 6(c) demonstrate that the quantity of protein loaded increased as hydrophilicity of the material increased. Finally, a power of 100 W oxygen plasma within a vacuum of 40–100 Pa for 1 min were chosen for surface treatment to achieve maximum protein loading.

3.4.2. Protein release

Using the optimal surface treatment conditions described above, the 3D-printed cervical implants were surface-treated and loaded with JB protein. The release of JB proteins from implants of different porosities is displayed in figures 7(a) and (b). The JB protein was released from the implants extremely quickly over the first 4 h, approximately 70% of the total quantity loaded. The slowest release rate was observed in implants with a wire spacing of 0.8 mm, in which the protein was continuously released for 20 h. Conversely, implants fabricated using a 1.6 mm wire spacing exhibited the fastest protein release rate, with almost all the loaded protein released within just 8 h. It is worth mentioning that the rate of protein release increased as fabrication wire spacing increased, probably due to the increased porosity. Furthermore, according to figure 7(c), the quantity of loaded protein (M) exhibited a linear negative correlation with measured porosity of the cervical implants, as follows:

$$M = -71.121\eta_{measured\,porosity} + 81.109,\ R^2 = 0.9929. \quad (8)$$

In order to determine whether the released JB protein could inhibit HPV, we incubated HPV pseudovirus, Hela cells and release solution for 16 h, and then tested the antiviral activity. As shown in figure 7(d), compared with the original protein

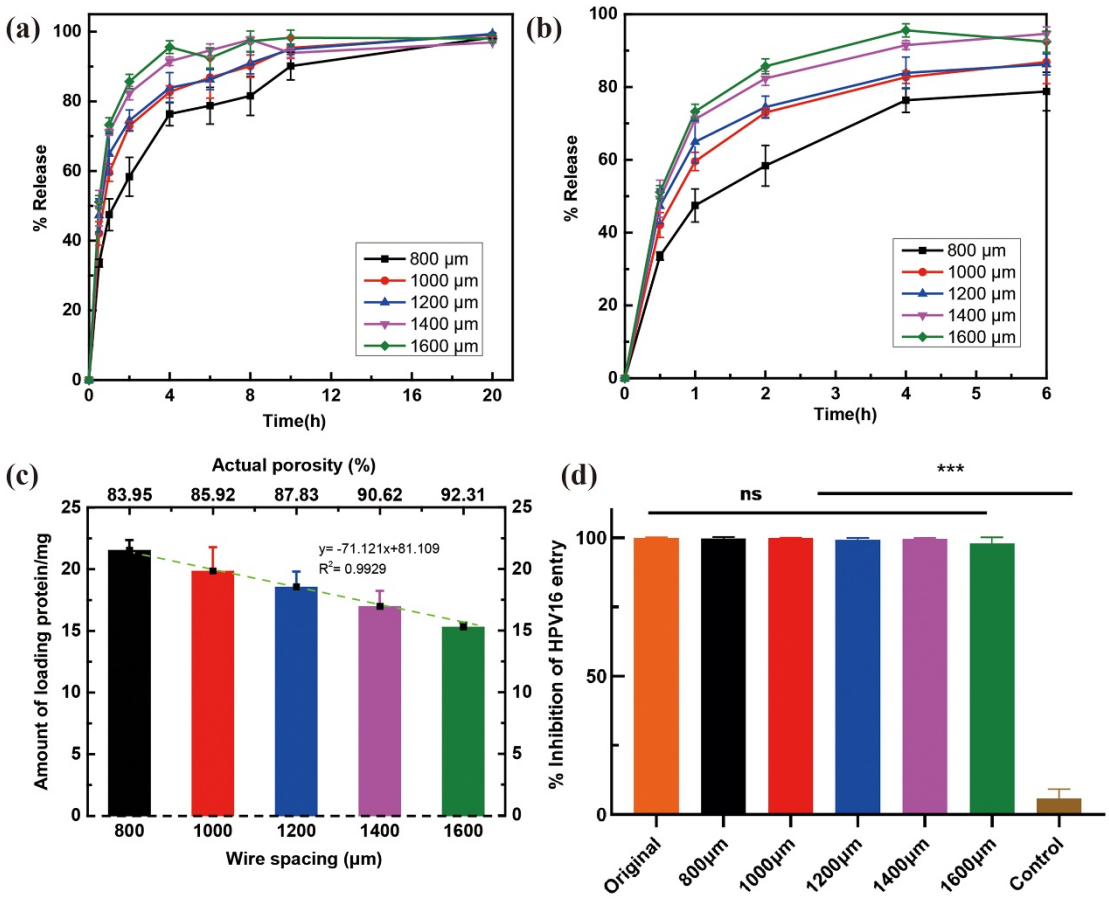

Figure 7. JB protein release profiles in PBS. (a) JB protein release profile until 20 h; (b) JB protein release profile from 0 h to 10 h; (c) the amount of JB protein loading on cervical implants with different wire spacing; (d) the inhibition effect against HPV pseudovirus before and after the protein releasing. ($p \leq 0.05$, $n = 3$).

before releasing, the released JB protein could still validly inhibit HPV pseudovirus from entering host cells with no reduced activity, indicating that the loading process do not influence the bioactivity of anti-HPV protein.

4. Discussion

After the conization in early stage cervical cancer, relapse occurrs in 13% of patients and 86% was local, since 10%–20% of acute HPV infections persistently attack host cells [44, 45]. What's more, considering the partial tissue defect caused by the surgery, it is necessary to provide patients with tissue repair as well as effective anti-HPV infection. Based on clinical data and the physical characteristics of the cervix, we utilized LDM technology to construct a biomimetic cervical implant that was capable of drug release. Pores at two hierarchical levels were successfully created that modified both the mechanical properties and drug loading and releasing characteristics. The materials underwent a variety of experimental characterization tests and the effects of different porosities on structural properties were examined. Due to the high elasticity of polyurethane and the porous structure, the 3D-printed constructs exhibited mechanical properties comparable to physiological tissue, with a compressive modulus of 0.06–0.25 MPa and elongation at break of 100%–200%. The properties of the 3D-printed constructs in supporting cell adhesion and growth were confirmed via cytotoxicity and cytocompatibility tests. The protein release profiles demonstrated that an increase in porosity accelerated the release of the protein. The association between porosity and quantity of drug loaded on the cervical implants was found to be a linear negative correlation. Moreover, the released JB protein could still effectively inhibit HPV pseudovirus from entering host cells with no reduced activity.

Cervix tissue is relatively homogeneous, composed principally of extracellular matrix (up to 90% collagen) and a small number of cells, with high elasticity [40, 46]. Considering the characteristics of cervix tissue and the need for future transplantation, polyurethane was chosen as the material for 3D printing due to its common use in tissue engineering applications and authorization by the United States Food and Drug Administration in clinical applications [47]. Polyurethane is polymerized from polyols (polyethers or polyesters), isocyanates, and chain extenders (diols and amines) and -NHCOO- (carbamate). The carbamate in the polyurethane

Table 2. Fit parameters for the release of JB protein from cervical implants of different porosities based on Weibull equation.

	Weibull equation $R_n = 100(1 - \exp\left(-(t/\tau)^d\right)$				
Wire spacing	Theoretical macro-porosity (%)	Actual porosity (%)	τ	d	R^2
800 μm	50	83.95 ± 5.07	1.624 ± 0.079	0.547 ± 0.031	0.99307
1000 μm	60	85.92 ± 2.25	1.172 ± 0.042	0.524 ± 0.028	0.99567
1200 μm	66.7	87.83 ± 4.23	1.045 ± 0.041	0.466 ± 0.030	0.99467
1400 μm	71.4	90.62 ± 1.39	0.897 ± 0.057	0.580 ± 0.059	0.9906
1600 μm	75	92.31 ± 1.59	0.834 ± 0.057	0.651 ± 0.073	0.9913

macromolecular chain is similar in polarity to the amide bond in the main extracellular component (collagen, elastin and proteoglycans, etc) of the cervix tissue, therefore, it is expected to have good biocompatibility with native tissue [48], as evidenced by biocompatibility test. Additionally, cervix tissue has excellent mechanical properties, being able to withstand incredibly large deformations and nevertheless remain strong. Through transvaginal ultrasonography, the deformation rate of the cervix during pregnancy is 23.7% ~ 54.4% [49, 50]. A wholesome cervix plays a vital role in maintaining intrauterine pressure during pregnancy [51], which defines the property of a printed cervical implants with good stretchability. In current study, tensile and compressive tests demonstrated that printed 3D constructs had an elongation at break of 100% to 200%, indicating that cervical implants exceeded deformation rates experienced during pregnancy and could contribute to a reduction in preterm birth rates. More importantly, the mechanical strength of the structure could be adjusted through a porosity change [52], which could be achieved by adjusting macropores with controlled size (equation (1)). Combined with the flexible change of digital model, cervical implants with specific macroscopic shape and mechanical properties could be tailored according to the physiological characteristics of individual patient.

The 3D-printed cervical implants in this research were not only suitable for tissue repair, they also functioned as a drug release system against the HPV virus. In order to maintain the activity of the protein, drug loading on the cervical implants was conducted using adsorption in this study. The protein solution entered the pores inside the constructs by negative pressure to enhance loading capacity. Results about the antiviral activity of released JB protein have proved that this loading method effectively maintain the protein bioactivity. In this study, LDM integrated with freeze-drying was employed to fabricate the cervix tissue implants with pores at two hierarchies, as confirmed by SEM. Macro-pores with a diameter of a few hundred microns were controlled by wire spacing, and micro-pores of 1–10 microns formed in each filament after freeze-drying. The formation of these micropores resulted in a higher specific surface area, which in turn leaded to higher drug dosages and loading efficiency [53]. Additionally, the surface area of the cervical implants could be regulated by the macropososity and the macroporosity could be controlled precisely through a change in wire spacing (equations (1), (2), (7)). As a result, the drug dosage load on cervical implants could also be controlled accurately, as confirmed by the linear relationship between porosity and drug loading capacity (equation (8)).

Comparing the protein release profiles of cervical implants with different porosities, it is noticeable that the rate of protein release increased with increasing porosity. The release kinetics of proteins are primarily determined by the adsorption-desorption equilibria in solution [54]. Based on the Weibull model, protein release followed an exponential relationship with duration of immersion with high correlation coefficients for all cervical implants of different porosities (table 2). The value of Weibull constant d for all cervical implants was less than 0.75, suggesting that protein release was controlled by Fickian diffusion [39]. According to the relationship between the Weibull model and release kinetics, the Weibull constant d is related to the diffusion coefficient, the specific surface area and the medium diffusion path [55]. Therefore, differences in release kinetics may be related to different structural properties of the cervical implants, such as porosity, surface area, and pore distribution [54]. In addition, the release kinetics parameter τ decreased as porosity increased, also suggesting that release rate increased as porosity increased. Consequently, protein release could be controlled through a change in wire spacing of the constructs, considering that porosity is largely determined by the wire spacing.

When the reproductive system is weak after the surgery, the dissociative viruses near the cervix, which cannot be removed through the conization, will be inhibited from entering the host cells by short-term release of the JB protein. However, previous research found that the median recurrence time for cervical cancers was 15.54 months [56], so the protein release in one day may not be long enough to completely eradicate all potential HPV virus in the vagina. Since the protein was only adsorbed on the surface of the material by intermolecular forces, this loose binding resulted in rapid release of the protein. In future research, we plan to directly mix the protein solution with the printed material or prepare the protein as a hydrogel to fill the pores in the cervical

implant to achieve prolonged release time. Additionally, the cervix is surrounded by viscous matrix and collagen *in vivo* [57], an environment different from the PBS buffer used in the *in vitro* release experiments. In future, it would be necessary to develop an *in vitro* release system that simulates more closely the *in vivo* environment to obtain a more accurate release profile.

5. Conclusions

In this study, cervix tissue implants with releasable antivirus protein were designed from clinical data and fabricated from polyurethane using LDM technology. By adjusting the wire spacing, 3D-printed cervical implants with different porosities were fabricated. As suggested by the mechanical tests, printed 3D constructs exhibited mechanical properties comparable to physiological cervix tissue with a compressive modulus of 0.06–0.25 MPa, capable of 1–2 times deformation. The constructs were also found to support cell adhesion and growth, according to cytotoxicity and cytocompatibility tests. Anti-HPV protein was successfully loaded onto the constructs and a linear negative correlation observed between construct porosity and dosage of loaded protein. Moreover, the release profiles fitted the Weibull model, demonstrating that increased porosity accelerated the rate of protein release. Most importantly, the released protein could still validly inhibit HPV pseudovirus from entering host cells with no reduced activity. These results suggest that the 3D-printed cervical implants could potentially contribute to tissue repair after conization and block HPV infection by protein release.

Acknowledgments

This work was supported by the National Natural Science Foundation of China No. 51805294, the Science and Technology Innovation Projects in Shanxi Transition Comprehensive Reform Demonstration Zone No. 2018KJCX05, the Tsinghua University Initiative Scientific Research Program No. 20197050024, the Beijing Natural Science Foundation through project No. 3184049, Strategic Priority Program (SPP) on Space Science No. XDA15014300, and the 111 Project No. G2017002. The authors give special thanks to Shanxi Jingbo Biological Pharmaceutical Co., Ltd for research support, and also acknowledge the valuable comments and time spent by referees to improve this manuscript.

ORCID iDs

Chenjia Zhao https://orcid.org/0000-0002-0923-9902
Yuan Pang https://orcid.org/0000-0003-3205-0830

References

[1] Diaz-Padilla I, Monk B J, Mackay H J and Oaknin A 2013 Treatment of metastatic cervical cancer: future directions involving targeted agents *Crit. Rev. Oncol. Hematol.* **85** 303–14
[2] Kessels S J M, Marshall H S, Watson M, Braunack-Mayer A J, Reuzel R and Tooher R L 2012 Factors associated with HPV vaccine uptake in teenage girls: A systematic review *Vaccine* **30** 3546–56
[3] Altobelli E and Lattanzi A 2015 Cervical carcinoma in the European Union: an update on disease burden, screening program state of activation, and coverage as of March 2014 *Int. J. Gynecol. Cancer* **25** 474
[4] Zhang M F, Fan J B and Shuai C Q 2006 Clinical analysis of two operation ways of cervical conization *Pract. Clin. Med.* **8** 104–105,108
[5] Martin-Hirsch P P, Paraskevaidis E and Kitchener H C 1999 Surgery for cervical intraepithelial neoplasia *Cochrane Database Syst. Rev.* **3** CD001318
[6] van de Vijver A, Poppe W, Verguts J and Arbyn M 2010 Pregnancy outcome after cervical conisation: a retrospective cohort study in the Leuven University Hospital *BJOG: Int. J. Obstet. Gynaecol.* **117** 268–73
[7] Freitas A C D, Gurgel A P A D, Chagas B S, Coimbra E C and Amaral C M M D 2012 Susceptibility to cervical cancer: an overview *Gynecol. Oncol.* **126** 304–11
[8] Silvano C *et al* 2003 Factors predicting human papillomavirus clearance in cervical intraepithelial neoplasia lesions treated by conization *Gynecol. Oncol.* **90** 358–65
[9] Lavik E and Langer R 2004 Tissue engineering: current state and perspectives *Appl. Microbiol. Biotechnol.* **65** 1–8
[10] Chapekar M S 2015 Tissue engineering: challenges and opportunities *J. Biomed. Mater. Res.* A **53** 617–20
[11] Spector M 2006 Biomaterials-based tissue engineering and regenerative medicine solutions to musculoskeletal problems *Swiss. Med. Wkly.* **136** 293–301
[12] Jeng L, Hsu H-P and Spector M 2013 Tissue-engineered cartilaginous constructs for the treatment of caprine cartilage defects, including distribution of laminin and type IV collagen *Tissue Eng.* A **19** 2267–74
[13] Griffith L G and Gail N 2002 Tissue engineering–current challenges and expanding opportunities *Science* **295** 1009–14
[14] Mironov V, Boland T, Trusk T, Forgacs G and Markwald R R 2003 Organ printing: computer-aided jet-based 3D tissue engineering *Trends Biotechnol.* **21** 157–61
[15] Boland T, Xu T, Damon B and Cui X 2006 Application of inkjet printing to tissue engineering *Biotechnol. J.* **1** 910–7
[16] Seyednejad H, Gawlitta D, Kuiper R V, Bruin A D, Nostrum C F V, Vermonden T, Dhert W J A and Hennink W E 2012 *In vivo* biocompatibility and biodegradation of 3D-printed porous scaffolds based on a hydroxyl-functionalized poly(ε-caprolactone) *Biomaterials* **33** 4309–18
[17] Rodríguez-Dévora J I, Zhang B, Reyna D, Shi Z D and Xu T 2012 High throughput miniature drug-screening platform using bioprinting technology *Biofabrication* **4** 035001
[18] Xu T, Baicu C, Aho M, Zile M and Boland T 2009 Fabrication and characterization of bio-engineered cardiac pseudo tissues *Biofabrication* **1** 035001
[19] Lee V K, Lanzi A M, Ngo H, Yoo -S-S, Vincent P A and Dai G 2014 Generation of multi-scale vascular network system within 3D hydrogel using 3D bio-printing technology *Cell. Mol. Bioeng.* **7** 460–72
[20] van Ijsseldijk E A, Valstar E R, Stoel B C, Nelissen R G H H, Baka N, van't Klooster R and Kaptein B L *et al* 2016 Three dimensional measurement of minimum joint space width in the knee from stereo radiographs using statistical shape models *Bone Joint Res.* **5** 320–7
[21] Ruiters S, Sun Y, Jong S D, Politis C and Mombaerts I 2016 Computer-aided design and three-dimensional printing in the manufacturing of an ocular prosthesis *Br. J. Ophthalmol.* **100** 879–81

[22] Morrison R J, Nasser H B, Zopf D A, Flanagan C L, Wheeler M, Green G E and Hollister S *et al* 2014 Biomechanical properties and effect on tracheobronchial growth of 3-D printed bioresorbable airway splints for treating tracheobronchomalacia *Tissue Eng.* A **20** S24
[23] Sun W, Li J, Li Q, Li G and Cai Z 2011 Clinical effectiveness of hemipelvic reconstruction using computer-aided custom-made prostheses after resection of malignant pelvic tumors *J. Arthroplasty* **26** 1508–13
[24] Su A P, Sang J L, Lim K S, Bae I H, Lee J H, Wan D K, Jeong M H and Park J-K *et al* 2015 *In vivo* evaluation and characterization of a bio-absorbable drug-coated stent fabricated using a 3D-printing system *Mater. Lett.* **141** 355–8
[25] Hung K-C, Tseng C-S, Dai L-G and Hsu S-H 2016 Water-based polyurethane 3D-printed scaffolds with controlled release function for customized cartilage tissue engineering *Biomaterials* **83** 156–68
[26] Xing J F, Zheng M L and Duan X M 2015 Two-photon polymerization microfabrication of hydrogels: an advanced 3D printing technology for tissue engineering and drug delivery *Chem. Soc. Rev.* **44** 5031–9
[27] Goyanes A, Det-Amornrat U, Wang J, Basit A W and Gaisford S 2016 3D scanning and 3D printing as innovative technologies for fabricating personalized topical drug delivery systems *J. Control. Release* **234** 41–48
[28] Xu M, Li Y, Suo H, Yan Y, Liu L, Wang Q, Ge Y and Xu Y *et al* 2010 Fabricating a pearl/PLGA composite scaffold by the low-temperature deposition manufacturing technique for bone tissue engineering *Biofabrication* **2** 025002
[29] Liu L, Xiong Z, Yan Y, Hu Y, Zhang R and Wang S 2007 Porous morphology, porosity, mechanical properties of poly (α-hydroxy acid)–tricalcium phosphate composite scaffolds fabricated by low-temperature deposition *J. Biomed. Mater. Res.* A **82** 618–29
[30] Neurath A R, Jiang S, Strick N, Lin K, Li Y Y and Debnath A K 1996 Bovine beta-lactoglobulin modified by 3-hydroxyphthalic anhydride blocks the CD4 cell receptor for HIV *Nat. Med.* **2** 230
[31] Lu L, Yang X, Li Y and Jiang S 2013 Chemically modified bovine beta-lactoglobulin inhibits human papillomavirus infection *Microbes Infect.* **15** 506–10
[32] Guo X *et al* 2016 A randomized open-label clinical trial of an anti-HPV biological dressing (JB01-BD) administered intravaginally to treat high-risk HPV infection *Microbes Infect.* **18** 148–52
[33] Guo X, Qiu L, Wang Y, Wang Y, Meng Y, Zhu Y, Lu L and Jiang S 2016 Safety evaluation of chemically modified beta-lactoglobulin administered intravaginally *J. Med. Virol.* **88** 1098–101
[34] Zhang T F, Ke-Ke X U, Huang Z X, Min D U, Zhang J J Liao S *et al* 2008 Clinical analysis of the effect of cervical conization on fertility and pregnancy outcome *Chin. J Endoscopy* **42** 1195–97
[35] Kurman R J, Elleson L H and Ronnett B M 2002 *Blaustein's Pathology of the Female Genital Tract* (New York: Springer) (https://doi.org/10.1007/978-1-4757-3889-6)
[36] Chen W, Liu Y, Zhang F and Qingxi H U 2013 The method of path planning for the regenerated bone-scaffold preparation based on additive manufacturing *J. Mech. Eng.* **49** 12
[37] Aksoy P, Abban C Y, Kiyashka E, Qiang W and Meneses P I 2014 HPV16 infection of HaCaTs is dependent on β4 integrin, and α6 integrin processing *Virology* **449** 45–52
[38] Li W, Zhou J and Xu Y 2015 Study of the *in vitro* cytotoxicity testing of medical devices *Biomed. Rep.* **3** 617–20
[39] Kosmas K, Panos A and Panos M 2003 A reappraisal of drug release laws using Monte Carlo simulations: the prevalence of the Weibull function *Pharm. Res.* **20** 988–95
[40] Jørgensen K and Jacobsen L 1992 Factorial design used for ruggedness testing of flow through cell dissolution method by means of Weibull transformed drug release profiles *Int. J. Pharm.* **88** 23–29
[41] Papadopoulou V, Kosmidis K, Vlachou M and Macheras P 2006 On the use of the Weibull function for the discernment of drug release mechanisms *Int. J. Pharm.* **309** 44–50
[42] Surviladze Z, Dziduszko A and Ozbun M A 2012 Essential roles for soluble virion-associated heparan sulfonated proteoglycans and growth factors in human papillomavirus infections *PLoS Pathog.* **8** e1002519
[43] Kwak K, Jiang R, Wang J W, Jagu S, Kirnbauer R and Roden R B 2014 Impact of inhibitors and L2 antibodies upon the infectivity of diverse alpha and beta human papillomavirus types *PLoS One* **9** e97232
[44] Tomao F, Maruccio M, Preti E P, Boveri S, Ricciardi E, Zanagnolo V and Landoni F 2017 Conization in early stage cervical cancer: pattern of recurrence in a 10-year single-institution experience *Int. J. Gynaecol. Cancer* **27** 1001–8
[45] Hua C, Zhu Y, Wu C, Si L, Wang Q, Sui L and Jiang S 2019 The underlying mechanism of 3-hydroxyphthalic anhydride-modified bovine beta-lactoglobulin to block human papillomavirus entry into the host cell *Frontiers Microbiol.* **10** 2188
[46] Nott J P, Bonney E A, Pickering J D and Simpson N A B 2016 The structure and function of the cervix during pregnancy *Transl. Res. Anat.* **2** 1–7
[47] United States Food & Drug Adminstration 2012 UD identification *Regulation of Medical Devices*
[48] Wang D Q, Wei L I, Liu X D and Huang Q S 2006 Application and research advances in medical polyurethane *Mod. Chem. Ind.* **26** 100–2
[49] Parra-Saavedra M, Gómez L, Barrero A, Parra G, Vergara F and Navarro E 2011 Prediction of preterm birth using the cervical consistency index *Ultrasound Obstet. Gynecol.* **38** 44–51
[50] Xiao-Hua L I, Jing-Ping L I, Hua X U, Wang S C, Zhou Y and Ultrasound D O 2017 Value of transvaginal ultrafast shear wave elastography imaging in the diagnosis of cervical carcinoma and precancerous lesions *Chin. Gen. Pract.* **20** 2285–88
[51] Baah-Dwomoh A, Mcguire J, Vita R D and Tan T 2016 Mechanical properties of female reproductive organs and supporting connective tissues: a review of the current state of knowledge *Appl. Mech. Rev.* **68** 060801
[52] Wu S, Liu X, Yeung K W, Liu C and Yang X 2014 Biomimetic porous scaffolds for bone tissue engineering *Mater. Sci. Eng.* R **80** 1–36
[53] Yu Y, Fu F, Shang L, Cheng Y, Gu Z and Zhao Y 2017 Bioinspired helical microfibers from microfluidics *Adv. Mater.* **29** 1605765
[54] Gbureck U, Vorndran E, Müller F A and Barralet J E 2007 Low temperature direct 3D-printed bioceramics and biocomposites as drug release matrices *J. Controlled Release* **122** 173–80
[55] Li B, Brown K V, Wenke J C and Guelcher S A 2010 Sustained release of vancomycin from polyurethane scaffolds inhibits infection of bone wounds in a rat femoral segmental defect model *J. Control. Release* **145** 221–30
[56] Wang H, Zhu L, Lu W, Xu H, Yu Y and Yang Y 2013 Clinicopathological risk factors for recurrence after neoadjuvant chemotherapy and radical hysterectomy in cervical cancer *World J. Surg. Oncol.* **11** 301
[57] Danforth D N, Veis A, Breen M, Weinstein H G, Buckingham J C and Manalo P 1974 The effect of pregnancy and labor on the human cervix: changes in collagen, glycoproteins, and glycosaminoglycans *Am. J. Obstet. Gynecol.* **120** 641–51